THE RESPONSE OF THE EQUATORIAL TROPOSPHERIC OZONE TO THE MADDENJULIAN OSCILLATION IN TES SATELLITE OBSERVATIONS AND CAM-CHEM MODEL SIMULATION

A Thesis

Presented to the Faculty of the Graduate School

of Cornell University

in Partial Fulfillment of the Requirements for the Degree of

Master of Science

by

Wenxiu Sun

January 2015

ABSTRACT

The Madden-Julian Oscillation (MJO) is the dominant form of the atmospheric intra-seasonal oscillation, manifested by slow eastward movement (about 5 m/s) of tropical deep convection. This study investigates the MJO's impact on equatorial tropospheric ozone (10N-10S) in satellite observations and chemical transport model (CTM) simulations. For the satellite observations, we analyze the Tropospheric Emission Spectrometer (TES) level-2 ozone profile data for the period of Jan 2004 to Jun 2009. For the CTM simulations, we run the Community Atmosphere Model with chemistry (CAM-chem) driven by the GOES-5 analyzed meteorological fields for the same data period as the TES measurements. Our analysis indicates that the behavior of the Total Tropospheric Column (TTC) ozone at the intraseasonal time scale is different from that of the total column ozone, with the signal in the equatorial region comparable with that in the subtropics. The model simulated and satellite measured ozone anomalies agree in their general pattern and amplitude when examined in the vertical cross section (the average spatial correlation coefficient among the 8 phases is 0.63), with an eastward propagation signature at a similar phase speed as the convective anomalies (5 m/s). The model ozone anomalies on the intraseasonal time scale are about five times larger when lightning emissions of NOx are included in the simulation than when they are not. Nevertheless, large-scale advection is the primary driving force for the ozone anomalies associated with the MJO. The variability related to the MJO for ozone reaches up to 47% of the total variability (ranging from daily to interannual), indicating the MJO should be accounted for in simulating ozone perturbations in the tropics.

BIOGRAPHICAL SKETCH

Wenxiu Sun is a PhD student studying Atmospheric Science in Cornell. She majored in Atmospheric Science at Nanjing University in China. Previously she interned in Department of Economic and Social Affairs of the United Nations.

This document is dedicated to all Cornell graduate students.

ACKNOWLEDGEMENTS

The author would like to give her most sincere thanks to Professor Hess, Peter, who advises her to finish this work. The author would also like to acknowledge Dr. Tian, Baijun, Professor Mahowald, Natalie and Professor Chen, Gang for their suggestions when reviewing this paper. Many thanks to Daniel Ward, Benjamin Brown-Steiner, Huang Yang, and Chengji Liu for their helpful discussions.

TABLE OF CONTENTS

LIST OF TABLES

LIST OF FIGURES

CHAPTER 1

INTRODUCTION

Tropospheric ozone is key in governing the tropospheric oxidation capacity through its role in producing hydroxyl (OH) radicals (Lelieveld and Dentener, 2000), the primary chemical sink for many chemical pollutants. Tropical ozone is of particular importance, as tropical OH removes approximately 85% of the methane molecules emitted in the atmosphere (e.g., Logan et al., 1981). Tropospheric ozone is also important in regulating the radiative forcing of climate (Worden et al., 2008, Lacis et al., 1990) with suggestions that the tropics are of particular importance (Houghton et al., 2001). However, the tropical tropospheric ozone distribution and variability have not been well documented and characterized, especially on the intraseasonal time scale (e.g., Thompson et al., 2003). This is true in the observations, as well as in model simulations, where the focus has been on the climatology or seasonal variation of the tropospheric total column ozone in the tropics. This study investigates the dominant form of the intra-seasonal oscillation, the Madden Julilian Oscillation's (MJO) (Madden and Julian, 1972) impact on equatorial tropospheric ozone (10N-10S) in satellite observations and in chemical transport model (CTM) simulations.

The MJO is characterized by slowly eastward-propagating, large-scale oscillations in the tropical deep convection and baroclinic wind field, especially over the warmest tropical waters in the equatorial Indian and western Pacific Oceans (e.g., Madden and Julian, 1971, 1972). In addition to its impacts on the global weather and climate (Lau and Waliser, 2012), it has recently been recognized that the MJO can also affect the atmospheric chemical composition, such as ozone, aerosols, carbon monoxide (CO) and carbon dioxide (CO_2), as

summarized in recent reviews (Tian and Waliser, 2011). For example, the MJO can impact the total column ozone (TCO). The associated TCO intra-seasonal anomalies are about ± 10 Dobson Unit (DU) and comparable to the TCO variability on annual and inter-annual time scales associated with ENSO, the QBO and the solar cycle (Tian et al., 2007). The MJO impacts the TCO mainly through its impact on the vertical movement of tropopause. Partial ozone intra-seasonal anomalies maximize approximately in the lower stratosphere between 30-200 hPa and account for more than 50% of the TCO anomalies (Li et al., 2012). The TCO intra-seasonal anomalies are mainly over the Pacific and eastern hemisphere and extend from the subtropics to the northern extra-tropics and the Arctic (Tian et al., 2007, Li et al., 2013).

The MJO can also impact the tropospheric ozone, especially near the equator (e.g., Ziemke and Chandra, 2003, Ziemke et al., 2007, Cooper et al., 2013). It was found that the equatorial tropospheric column ozone as well as equatorial upper tropospheric ozone decreases during the enhanced phase of MJO events indicating the MJO can directly impact the equatorial tropospheric column ozone and upper tropospheric ozone. These previous studies have shed light into the MJO's impacts on the tropospheric ozone but large uncertainties may exist in their calculation of the tropospheric column ozone as it was calculated as a small residual of two large quantities, i.e., TOMS or OMI TCO and UARS or Aura MLS stratospheric column ozone. Thus, satellite ozone data with vertical resolution in the troposphere will better refine the impact of the MJO on tropospheric ozone.

In addition, model simulations also provide an essential tool in understanding how the MJO influences tropospheric ozone. During the MJO, large-scale

overturning zonal circulations extend vertically through the troposphere and connect the regions of enhanced and suppressed convection (Zhang, 2005). This large-scale circulation and the deep convection associated with the MJO propagate together, making it difficult to separate their individual effects on the tropospheric ozone solely from the observations. However, model simulations can better isolate the different components of the MJO.

There are three ways that convection associated with the MJO can affect tropical tropospheric ozone. First, convection affects ozone by vertical mixing of ozone itself. Convection lifts lower tropospheric air to the upper troposphere where the ozone lifetime is longer, while mass-balance subsidence mixes ozone-rich upper tropospheric air downwards to lower troposphere where the ozone lifetime is shorter (Lelieveld and Crutzen, 1994). This tends to decrease upper tropospheric ozone and the overall tropospheric column of ozone. Secondly, convection affects ozone by the vertical mixing of ozone precursors that influence tropospheric ozone chemical production and destruction. Where there are short-lived surface ozone precursor sources, such as isoprene (C_5H_8), NOx ($NO+NO_2$), carbon monoxide (CO) and hydrocarbons over polluted regions, convection significantly increases these precursor concentrations, and thus ozone, in the mid- and upper-troposphere at the expense of the lower tropospheric concentrations. For example, Lawrence et al. (2003) found that lofting of surface NOx is a significant driver of increases in ozone production over much of the tropospheric column in a chemical transport model. Third, lightning in the tropics is a major NOx source (Sauvage et al., 2007, Ziemke et al., 2009) directly associated with convection, with most NOx added to the upper troposphere (Pickering et al., 1998). Labrador et al. (2005) found that lighting increased peak tropical ozone enhancements between 200 and 700 hPa by 30%,

and peak OH enhancements by 100%. Variations of lightning flash rate associated with the MJO over the Maritime Continent were found to be up to 50% of the annual mean flash rate (Virts et al., 2011, 2013). Despite its importance lightning produced NOx is still very uncertain with global estimates ranging from 1-20 Tg (N)/yr (Lawrence et al., 1995, Price et al., 1997).

Previous model studies show inconsistencies of convection's net effect on ozone due to different chemistry and convective schemes used in the models. Lelieveld and Crutzen (1994) used a model with no NMHC (Non-Methane Hydrocarbon) chemistry and found convection caused a significant 20% decrease of total tropospheric ozone. Doherty et al. (2005) also found convection reduced the global tropospheric ozone burden (by 13%) using a more complex Lagrangian chemistry-GCM (STOCHEM-HadAM3) with detailed NMHC chemistry. On the other hand, Lawrence et al. (2003), also using a complex CTM (MATCH-MPIC) with detailed NMHC chemistry, found vertical convective transport of ozone precursors outweighed the convective transport of ozone itself resulting in a 12% increase in tropospheric ozone due to convection.

Thus the dynamic (e.g., convection and large-scale circulation) versus chemical (ozone production/destruction due to ozone precursors, such as isoprene, NOx, hydrocarbons, and lightning) contribution to the tropospheric ozone variations related to the MJO is still unclear. In this study, we examine the response of tropospheric ozone to the MJO in the equatorial region and the factors that drive the response using recent tropospheric ozone satellite data (TES) and a chemical transport model (CAM-chem). Section 2 briefly describes the methodology. It includes a description of the chemical transport model and its analysis, as well as the satellite data sets used for model evaluation. Section 3 evalu-

ates the simulation of equatorial ozone climatology and the ozone MJO signal against TES ozone observations. Here we also examine the sensitivity of the simulation with respect to lightning and analyze the importance of various processes in determining the ozone changes during the MJO. Section 4 analyzes the structure and processes determining the equatorial MJO of ozone in the model and observations. The conclusions are given in Section 5.

CHAPTER 2

DATA AND METHOD

2.1 Satellite Measurements

The Level-2 (L2) ozone profiles measured by Tropospheric Emission Spectrometer (TES) from August 30, 2004 to June 4, 2009 (Beer et al., 2001, Jourdain et al., 2007, Worden et al., 2007) are used in this study. The TES instrument was launched in 2004 on the NASA Aura satellite into a sun-synchronous near-polar orbit with equatorial crossing times of 01:43 and 13:43 local solar time. TES is an infrared Fourier-transform spectrometer, covering the spectral range 650-3050 cm^{-1} (3.3-15.4 mm) (Beer, 2006). TES nadir observation have 0.1 cm^{-1} spectral resolution and a horizontal footprint of 5.3 km $\times$ 8.5 km. O_3 profiles are retrieved from the infrared channels covering the O_3 ν_3 band (1050 cm^{-1} or 9.6 mm) using a non-linear optimal estimation algorithm (Rodgers et al., 2000, Worden et al., 2004, Bowman et al., 2006) on 67 pressure levels between the surface and 5 hPa, with a vertical spacing of 0.7 km below 10 hPa. These infrared channels are most sensitive to O_3 at levels between 900 and 30 hPa with a vertical resolution of 6 km for clear sky scenes. The ozone profile estimates from TES have been compared with aircraft, in-situ, and model studies. TES ozone is biased high, particularly in the upper troposphere, by 3-10 ppb, compared to sondes (Nassar et al., 2008, Osterman et al., 2008, Worden et al., 2007) and lidar (Richards et al., 2008). When and where there are optically thick clouds, the TES retrieved O_3 profiles below the optically thick clouds comes mainly from the a priori O_3 profile because the retrieved O_3 information below the cloud tops can be very low (Kulawik et al., 2006, Eldering et al., 2008). The data used in this

study is based on V004 TES data, which is available at the NASA Langley Atmospheric Data Center (http://eosweb.larc.nasa.gov/). To identify the convective features of the MJO, we use the V6 3B42 Tropical Rainfall Measuring Mission (TRMM) precipitation products (Huffman et al., 2007).

2.2 Model

The global Community Atmosphere Model (CAM) with chemistry (CAM-chem), the atmosphere, land and chemical components of the Community Earth System model (CESM), is used to simulate the atmospheric chemistry and circulation associated with the MJO. Here we use CAM4 from the version 1.0.4 of the CESM. Since we are most interested in the model simulation of the tropospheric ozone variation given realistic dynamical forcing of the MJO (convection, precipitation and large-scale circulation), the CAM-chem was driven by Goddard Earth Observing System Model, Version 5 (GEOS-5) analyzed meteorological fields for the period Jan 2004 to Jun 2009 with the first 8 months used as spin up. The analysis date starts from Aug 31, 2004.

We perform two simulations with CAM-chem: one control simulation, and one simulation with no lightning emissions of NOx. The latter simulation allows us to understand the role of lightning in the tropospheric ozone.

CAM-chem and its various components are described in detail in Lamarque et al. (2012). Deep convection uses the parameterization of the Zhang-McFarlane approach (Zhang and McFarlane, 1995) with some modifications, and shallow convection follows Hack et al. (2006). The planetary boundary layer is represented using the Holtslag and Boville (1993) parameterization. The

model has a 1.9°×2.5° horizontal resolution and 56 vertical levels to 4 hPa, and the vertical coordinate is a hybrid sigma pressure (Lamarque et al., 2012). The chemistry used in CAM-chem is adapted from MOZART-4 (including 85 gas-phase species, 12 bulk aerosol compounds, 39 photolysis and 157 gas-phase reactions (Emmons et al., 2010), by adding chemical reactions for C_2H_2, HCOOH, HCN and CH_3CN and minor changes to the isoprene oxidation scheme (Lamarque et al., 2012). Stratospheric chemistry is not explicitly represented, and ozone from the model top to 50 hPa uses input monthly-mean climatological ozone concentrations from 1950-2005 from WACCM simulations (Garcia et al., 2007). Between 50 hPa and 2 model levels above the tropopause (approximately 150 hPa) ozone is relaxed to the WACCM distribution with a 10-day relaxation time.

The anthropogenic emissions for most species are from the POET (Precursors of Ozone and their Effects in the Troposphere) database for 2000 (Granier et al., 2005). Anthropogenic emissions for SO_2 and NH_3 are taken from the EDGAR-FT2000 and EDGAR-2 databases (http://www.mnp.nl/edgar/). Aircraft emissions of NO, CO and SO_2 from scheduled, charter, general aviation and military traffic for 1999 are included (Baughcum et al., 1996, 1998, Mortlock and Van Alstyne, 1998, Sutkus et al., 2001) and have global annual totals of 0.63 Tg yr^{-1} (1.35 Tg N yr^{-1}) for NO, 1.70 Tg yr^{-1} for CO and 0.16 Tg yr^{-1} for SO_2 (Emmons et al., 2010). Monthly average biomass burning emissions for each year come from the Global Fire Emissions Database, version 2 (GFED-v2), which is currently available for 1997-2007 (van der Werf et al., 2006). Emissions for species not provided in GFED (e.g., individual volatile organic compounds as specified in MOZART-4, SO_2, and NH_3) are determined by scaling the GFED CO_2 emissions by the emission factors of Andreae and Merlet (2001) and updates to it (Granier et al., 2005), using the vegetation classification provided with GFED. The emissions of

NO from lightning are based on the Price and Rind parameterization (Price and Rind, 1992, Price et al., 1997), providing a global annual emission of 3-5 Tg (N) yr^{-1} (Lamarque et al., 2012). To fully exploit the advantage of using the earth system model, we use the land model to interactively calculate the emissions of biogenic hydrocarbons based on the MEGAN algorithm (Guenther et al., 2006).

To compare the simulated ozone with TES observations, the TES operator is applied to the simulation data. After extracting co-located spatial and temporal points from the simulation, the ozone is interpolated vertically to match the observed pressure levels of the satellite data, then adjusted using the a priori profiles and the averaging kernel matrices (jointly referred to as observation operator) to account for limited vertical resolution of observations and the impact of clouds (Kulawik et al., 2006).

Within the model simulation we separate the ozone tendency into various processes so as to understand how the ozone climatology is maintained and how the MJO changes the ozone distribution. In every grid box, the ozone change is attributed to the following tendency terms: advection (horizontal and vertical advection), deep convection, chemistry, shallow convection, and vertical diffusion.

$$\left(\frac{\partial O_3}{\partial t}\right) = \left(\frac{\partial O_3}{\partial t}\right)_{advection} + \left(\frac{\partial O_3}{\partial t}\right)_{deepconvection} + \left(\frac{\partial O_3}{\partial t}\right)_{chemistry} + \left(\frac{\partial O_3}{\partial t}\right)_{shallowconvection} + \left(\frac{\partial O_3}{\partial t}\right)_{verticaldiffusion} \tag{2.1}$$

Results (not shown) indicate that shallow convection and vertical diffusion

are much smaller than the other three terms, and are not further analyzed. The advective algortihm (the flux form of the semi-lagrangian scheme) does not readily allow the differentiation of advection into vertical and horizontal components.

2.3 Data Analysis

The analysis method is similar to that used in our previous studies (e.g., Tian et al., 2010, 2011, Li et al., 2012, 2013). To isolate the MJO signal in the satellite measured and model simulated data the average annual cycle of each field is first calculated and smoothed with a 30-day running average, then daily anomaly signals are obtained by subtracting the smoothed annual cycle from daily data. Finally the MJO signal is obtained by applying a 30 to 60 day bandpass filter to the daily anomalies. The daily MJO anomalies are sorted into 8 MJO phases according to the all-season real-time multivariate MJO (RMM) index, which is constructed using the combined EOF of the equatorial-mean (15S-15N) OLR, 200hPa and 850hPa zonal winds, and the leading two EOFs explain 25% of the variance of these fields (Wheeler and Hendon, 2004). This daily index characterizes the state of the MJO in terms of its amplitude and phase, where the latter divides the MJO cycle (typically about 40-55 days) into 8 phases, each roughly lasting about 6 days. Phase 1 represents developing positive rainfall anomalies in the western Indian Ocean, with the sequential progression to Phase 8 corresponding to the eastward propagation of positive rainfall anomalies across the eastern Indian Ocean, Maritime Continent, western Pacific, and onto the central/eastern Pacific Ocean (Hendon and Salby, 1994). In this study, composite MJO cycles of interested quantities, such as rainfall and O3, are pro-

duced by separately averaging together all daily anomaly values of the given quantity for each phase of the MJO, considering only strong amplitude events where $RMM_1^2 + RMM_2^2 > 1$. We restrict our analysis to the North Hemisphere (boreal) winter months (November to April) from 2004 to 2009 because the MJO signal is stronger when the Indo-Pacific warm pool is centered near the equator. When performing the model and TES comparison, we binned the data into 20° latitude (10°N-10°S) × 10° longitude bins to have sufficient daily data. The number of TES observations per lat/lon bin ranges from 0 to 8 per day and the average number of observations for all the bins of the 10S to 10N area is approximately 1-2 for each day.

CHAPTER 3

CLIMATOLOGICAL OZONE DISTRIBUTION

CAM-chem has been extensively evaluated (Lamarque et al., 2012). A comparison of the model against tropical ozonesondes suggests a positive surface bias of approximately 20-40% for all seasons, a good simulation throughout the mid-troposphere and a positive upper tropospheric bias above 400 hPa of approximately 40% from December through May (Lamarque et al., 2012). Here we analyze and evaluate the CAM-chem climatology in the equatorial region (10N-10S) for the months of Nov-Apr from 2004 to 2009.

3.1 Climatology of equatorial tropospheric ozone

CAM-chem simulated and TRMM measured tropical precipitation show good agreement both in their spatial distribution and magnitude. Climatological precipitation local maxima are found near 100E, 150E, and 60W both in the model simulation and satellite observations (Fig. 1), indicating strong convection at these longitudes. A local maximum of precipitation at 30E was found only in the model simulation but not in the TRMM data. The CAM-chem simulated ozone distribution with the TES averaging kernel applied and the TES ozone distribution are highly correlated (spatial correlation coefficient is 0.84 from 200 hPa to surface; Fig. 1). From 30-80E high ozone concentrations are evident throughout most of the depth of the troposphere in both model simulation and satellite measurements. Near 100E and 150E low ozone concentrations are evident throughout the depth of the troposphere in both model simulation and satellite measurements. They are associated with a precipitation maximum and

have been attributed to enhanced convection transporting low ozone concentrations from the oceanic boundary layer to the upper troposphere (Lelieveld et al., 2001). The precipitation maximum near 60W in the equatorial South America, however, is not associated with low upper tropospheric ozone concentrations in either the model simulation or the satellite measurements due probably to the high surface ozone concentration over land (see section 3.1.2). This may also be true for the local precipitation maximum and high upper tropospheric ozone concentrations near 30E over the equatorial Africa. However, there are some detailed differences between the CAM-chem model simulation and the TES satellite observations. For example, CAM-chem has a positive bias of ozone (~ 10 ppb) compared with TES (Fig. 1d) over the upper troposphere with the largest bias located near 90-60W. In the middle troposphere over the western Pacific (near 150E) and near the date line the model simulated ozone is generally less than the satellite measured (~ 10 ppb). In the boundary layer, the CAM-chem is positively biased compared with TES. The TES boundary layer ozone distribution is determined primarily by the apriori distribution and so may not reflect the actual ozone distribution there. The TES operator does not dramatically change the simulated ozone distribution (compare Fig. 1b and 1a), although the result of applying the TES operator is to increase the boundary layer ozone and reduce the upper tropospheric ozone (near the date line). The CAM-chem simulated ozone concentration with TES operator applied (Fig. 1b) is consistent with simulations using GEOS-Chem (Bowman et al., 2009). .

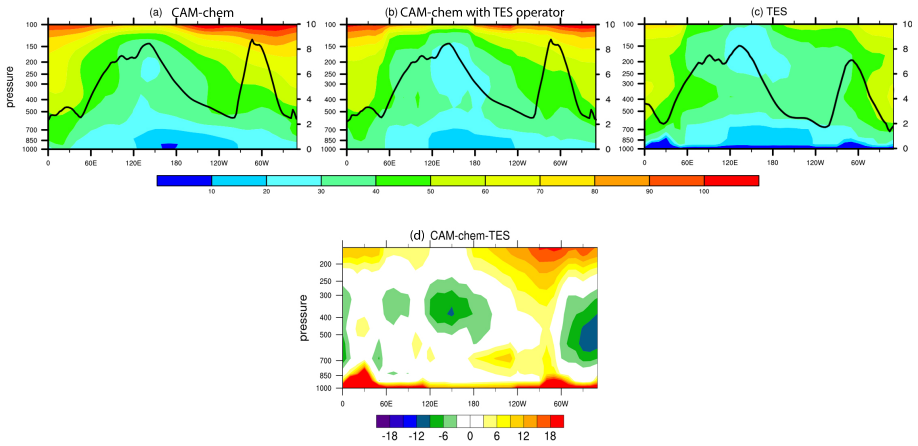

Figure 3.1: Climatology of tropospheric ozone (color, in ppb) during boreal winter (Nov-Apr) averaged between 10S to 10N for CAM-chem (a), CAM-chem with TES operator (b) and TES (c) and difference between CAM-chem and TES (d) with precipitation (lines, right axis, in mm/day) from CAM-chem (a,b) and TRMM (c).

3.2 The climatological tendency terms

In a climatological sense the net ozone tendency (Equation (1)) is close to zero. In the upper troposphere both advection and deep convection decrease ozone above 400-500 hPa as they transport depleted ozone upwards (Fig. 2). The pronounced convective ozone reductions generally occur in a sharply defined

layer from 300-500 hPa (approximately 7-10 km), which is lower than altitudes of 12-14 km (150-200 hPa) of strong tropical convection outflow suggested by Folkins and Martin (2005) and Randel and Jensen (2013). However, note that near 60W a convective signal is simulated at higher altitudes, near 200 hPa. The minimum deep convection tendencies near 30E, 90E, 160E and 60W near 400hPa colocate with the precipitation local maxima (Fig. 1). Above 300 hPa large-scale advection reduces the ozone concentrations everywhere, with the largest reductions above regions of strong convective ozone reductions (with the exception of 150E). The large reductions of ozone can be attributed to large-scale ascent above the level of maximum convection (Randel and Jensen, 2013). Chemical ozone production is generally positive above 400 hPa, with the strong positive ozone production coincident with regions of large advective ozone decreases, consistent with the results from Folkins et al. (2002, Fig. 14). Note that the tendency of chemistry and advection are opposed at the altitudes of 7-12km (400hPa to 200hPa).

In the lower troposphere transport generally increases the ozone concentration as ozone rich air subsides in the vicinity of deep moist convection (Lelieveld and Crutzen, 1994, Doherty et al., 2005). Positive convective transport is particularly noticeable below regions with pronounced negative convective transport at 400 hPa. An exception to the lower level convective increase of ozone occurs near 90-120E, a region where chemical ozone production is pronounced and convection decreases boundary layer ozone. Low-level ozone enhancements are also evident near 90W, associated with the subsiding motion associated with the Walker Circulation. Net chemical destruction generally balances the positive transport tendencies below approximately 600 hPa. In the boundary layer near 30E, 120E and 60W the net chemical production is positive, probably resulting

from the strong surface emissions in these regions.

3.3 The Climatological Role of Lightning

Lightning NOx emission is an important component of the tropical ozone budget. The largest model simulated lightning NOx sources occur near 30E, 100E, 150E and 60 W (Fig. 3b). These lightning NOx source local maxima all correspond to precipitation local maxima. These regions are also associated with the strong positive net chemistry tendencies in the upper troposphere (Fig. 2). Parameterized lightning NOx emissions are larger over land (30E-Africa, 60W-South America) and considerably reduced over the ocean (150E-western Pacific) and Maritime Continent (100E), consistent with observations (Price and Rind, 1992).

The ozone distribution in the control run (Fig. 1a) and the simulation where the lightning NOx emissions are turned off (Fig. 3a) are qualitatively similar, where both show a "wave-one" pattern with an ozone maximum over the tropical Atlantic and a minimum over the tropical Pacific; however, the simulation without lightning generally reduces ozone everywhere and in particular reduces the longitudinal and vertical tropical ozone gradients (Fig. 3b). The difference between the control run and the simulation with no lightning reaches up to 30 ppb in the upper troposphere near 60W and 10E (where the lightning NO source is maximum), consistent with the differences found by Sauvage et al. (2007, Fig. 6) but larger than the approximately 20 ppb differences suggested in Martin et al. (2002, Fig. 15). The largest differences between the simulations with and without lightning do not occur where the peak lightning NOx emis-

sions locate, indicating the relation between lighting NOx emissions and the ozone bias is not completely straightforward. The large lightning NOx source from 80W to 50E can explain the relatively high ozone concentration over the South America, Atlantic Ocean, and Africa. On the other hand, the relatively low lightning NOx emissions in the Pacific must be an important factor in maintaining the rather low upper tropospheric ozone concentrations there.

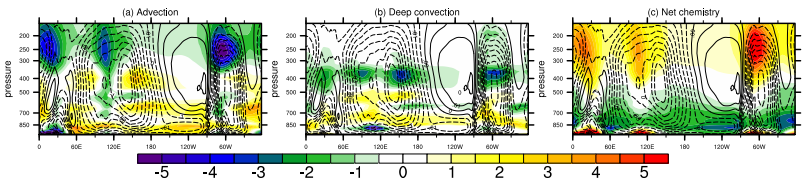

Figure 3.2: Vertical profile of the tropospheric climatology of the three major tendency terms (color shades, in ppb/day) for boreal winter (Nov-Apr) averaged between 10S to 10N: advection (a), deep convection (b) and net chemistry (c) with vertical velocity lines (dashed lines denoting negative values/upward motions and solid lines presenting the positive values/downward motions).

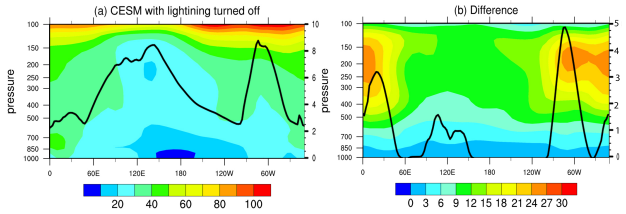

Figure 3.3: Tropospheric ozone climatology for boreal winter (Nov-Apr) averaged between 10S to 10N for (a) CAM-chem lightning turned off run (color, in ppb) with the precipitation (line, in mm/day) and (b) the difference between the control run and lightning turned off run (color, in ppb) with the lightning NOx source (line, in $1e^{-3}$TgN/yr).

CHAPTER 4

SIMULATED AND MEASURED MJO SIGNAL

In this section we discuss the MJO signal in equatorial tropospheric ozone in satellite observations and CAM-chem simulations and analyze the budget terms responsible for the model simulated MJO-related equatorial tropospheric ozone changes.

The region (45E-100E,10S-10N) over the Indian Ocean is chosen to look at the MJO-related tropospheric column ozone anomalies (deseasonalized 30-60 day bandpass filtered) time series from Nov 2004 to Jun 2009 (Fig. 4). The correlation of the CAM-chem simulated and TES observed tropospheric column ozone anomalies is 0.8, which is significant at the student's test 95% confidence level. The peak-to-peak variability reaches up to 4-5 DU, suggesting that MJO is an important process influencing the equatorial tropospheric ozone column.

4.1 MJO Signal in Total Tropospheric Column (TTC) Ozone

The patterns of simulated and measured TTC ozone anomalies and precipitation anomalies for the eight phases of the MJO (Wheeler and Hendon, 2004) are in overall agreement (Fig. 5) both in the tropics and the subtropics (the average spatial correlation coefficient is .658 for ozone and .762 for precipitation, both statistically significant). See Table 1 for the model-measurement spatial correlation coefficient for each phase). The positive precipitation anomalies (green lines), indicating the convection-active center, originates in western Indian Ocean in phase 1, and moves eastward to eastern Indian Ocean (phase

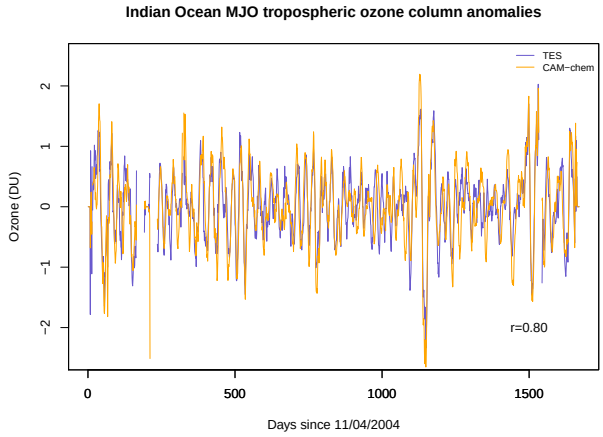

Figure 4.1: Time series of the 30-60 day band-pass filtered deseasonalized tropospheric ozone column anomalies (in DU) from TES and CAM-chem averaged over the Indian Ocean (45E-100E, 10S-10N).

2 and 3), Maritime Continent (phase 4 and 5), western Pacific (phase 6 and 7) and central/eastern Pacific Ocean in phase 8, consistent with the previous MJO studies (e.g., Hendon and Salby, 1994). While the magnitude of the model simulated and satellite measured ozone anomalies are in general agreement, the magnitude and the spatial scale of the precipitation anomalies in CAM-chem are smaller than that observed in TRMM. The magnitude of MJO-related TTC ozone anomalies in the equatorial region is comparable to that in the subtropics. On the other hand, Tian et al. (2007) shows the satellite derived MJO-related TCO anomalies are larger in the subtropics than in the equatorial region. This suggests the behavior of the TTC ozone on the intraseasonal time scale is different from that of the TCO, especially in the equatorial region. In Fig. 6 the vertical ozone anomaly pattern between 10N and 10S is analyzed in detail.

Table 4.1: Longitude-latitude (30S-30N) spatial correlation coefficients between modeled and measured ozone and precipitation anomalies, correlated for each phase of the MJO between CAM-chem and TES tropospheric ozone column (324 points) and CAM-chem and TRMM precipitation (4608 points). All correlation coefficients pass student's-t test at 95% confidence level.

Phase	Ozone	Precipitaion
1	0.565	0.759
2	0.676	0.775
3	0.699	0.789
4	0.725	0.765
5	0.614	0.782
6	0.632	0.763
7	0.710	0.727
8	0.641	0.740

4.2 Vertical Profiles of the MJO-related Tropospheric Ozone Anomalies

The phase of the precipitation anomalies in the model and measurements are in general agreement (Fig. 5, 6). Consistent with previous analyses (e.g., Zhang, 2005) the MJO convective signal is characterized by an eastward moving precipitation anomaly with greatest amplitude in the Western Pacific. A slight positive precipitation anomaly is observed over the equatorial central Indian Ocean (near 60E) in phase 1, it then becomes amplified and moves slowly eastward across the Maritime Continent and western equatorial Pacific in phases 2-6. It finally disappears over the central equatorial Pacific in phases 7-8. Sim-

ilarly, a slight negative precipitation anomaly is observed over the equatorial central Indian Ocean (near 60E) in phase 5, it then becomes amplified and moves slowly eastward across the Maritime Continent and western equatorial Pacific in phases 6-8-1-3. It finally disappears over the central equatorial Pacific in phase 4.

The vertical velocity anomaly fields derived from the GEOS-5 analyses (Fig. 6) are consistent with those derived from NCEP reanalysis data as given in Zhang and Mu (2005). The precipitation anomalies are clearly associated with pronounced anomalies in the vertical velocity consistent with previous studies (e.g., Jee-Hoon et al., 2008). Phases 1 through 6 are characterized by a generally strengthening upward vertical velocity anomaly moving slowly eastward, coincident with the positive precipitation anomaly. Weakened upward vertical velocities are located over the East Pacific for phases 7 and 8. Similar as the negative precipitation anomaly, the downward anomaly in vertical velocity, is identified over the central Indian Ocean in phase 5, and moves eastward from phase 6-3, before it finally weakens in phase 4 in the western hemisphere.

The MJO ozone anomalies in the upper level of the atmosphere (e.g., 200 hPa) (Fig. 6) are similar to the TTC ozone anomalies shown in Fig. 5 as the ozone change in the upper troposphere dominates that in the lower troposphere. The largest ozone anomalies occur in the Indian Ocean and western Pacific in association with the largest vertical velocity anomalies. The total and upper tropospheric ozone anomalies move eastward with the eastward propagation of the large-scale MJO convective and dynamical anomalies.

Viewed in the vertical the modeled and measured ozone anomalies generally agree in pattern and amplitude, with the average spatial correlation coefficient

0.63 for the 8 phases, which is significant at the 95% confidence level (Table 2 gives the correlation coefficients for each phase). In both the model simulation and satellite measurement a pronounced positive O_3 anomaly occurs in the Indian Ocean during phase 1 centered in the very upper troposphere over the region of the slightly positive rainfall anomaly and to the west of the negative rainfall anomaly. During phases 2-3 this positive O_3 anomaly shifts eastward and weakens considerably. In both the model simulation and satellite measurement the positive ozone anomaly in phase 1 over the Indian Ocean is replaced by a negative anomaly in phase 2 centered in the middle troposphere. During phases 2-6, this negative ozone anomaly shifts eastward and is coincident with or locates slightly to the west of the positive rainfall anomaly. During phases 6-8 the positive O_3 anomaly rebuilds over western portion of the equatorial domain. The ozone signal in the eastern portion of the domain propagates very little but is generally out of phase with the signal in the western portion of the domain. Model-measurement ozone discrepancies exist in sign near 30W for phase 1-4 and 8 and TES has a slightly larger signal for some phases (e.g., phase 7 over Indian Ocean). A detailed ozone budget is given in section 4.4.

Fig. 7 (left panel) shows the ozone anomalies from the model simulation without applying the TES operator. The difference in magnitude of the ozone anomalies associated with the MJO between Fig. 6 and Fig. 7 shows that the TES operator flattens the ozone anomalies and decreases the magnitude by 50%. The TES operator also changes the relative magnitude of the signal between phases. When the TES operator is applied only phases 1 and 8 are particularly enhanced, while the raw model output suggests the ozone signal is not considerably weaker during the other phases. Thus while the magnitude of the ozone anomaly with the TES operator appears to weaken considerably between

Table 4.2: Longitude-height (surface to 100 hPa) spatial correlation coefficients between modeled and measured ozone anomalies and longitudinal correlation coefficients between modeled and measured precipitation anomalies, correlated for each phase of the MJO between CAM-chem and TES tropospheric ozone column (936 points) and CAM-chem and TRMM precipitation (144 points). Fields are averaged from 10S to 10N. All correlation coefficients pass student's-t test at 95% confidence level.

Phase	Ozone	Precipitaion
1	0.779	0.940
2	0.603	0.973
3	0.616	0.975
4	0.696	0.965
5	0.676	0.979
6	0.524	0.976
7	0.400	0.957
8	0.802	0.910

phases 1 and 2, this is not apparent in the raw model simulations. Instead the positive ozone anomaly located near 60E during phase 1 moves eastward with little diminishment in amplitude until phase 4 in the raw model simulations, while to its west it is replaced by a pronounced negative anomaly with eastward propagation. In addition, the relationship between the downward vertical velocity and the positive ozone anomaly is much clearer and more consistent without the TES operator.

An MJO signal is also apparent in the lower troposphere when the TES operator is not applied, particularly in the western part of the domain. An eastward propagating negative anomaly is apparent from phases 1-5 below 500 hPa west

of the dateline, with an eastward propagating positive anomaly from phases 3-8. East of the dateline lower tropospheric anomalies are apparent but less distinct with a less distinct propagation. The upper and lower tropospheric MJO anomalies are often out of phase in the western part of the domain with an apparent east-to-west tilt. This can be traced to vertical differences in sign of the vertical velocity fields and their east-west tilt (e.g., Sperber, 2003).

4.3 Impact of Lightning on the MJO-related Tropospheric Ozone Anomaly

The comparison of MJO-related ozone anomalies between the control run and the lightning turned off run (without applying the TES operator) is given in Fig. 7. With the lightning turned on, the model-simulated ozone anomalies on the intraseasonal time scale are much larger, about 5 times bigger as those without lightning. However, a similar anomaly pattern is still present. The spatial correlation coefficient between the run with and without lightning is on average 0.89 for the 8 phases (significant at the 95% confidence level). This suggests while lightning and the associated chemistry act to enhance the MJO-related tropospheric ozone anomalies, they do not fundamentally change their vertical and horizontal structure.

4.4 MJO-related Tropospheric Ozone Tendencies

To explain the equatorial tropospheric ozone's response to the MJO, we calculate the 5 terms in Equation (1) using model results and we show the three major terms (advection, deep convection and net chemistry) in Fig. 8 (only phase 1, 3, 5, 7 are shown for simplicity). The total ozone tendency term explains the change between phases in Fig. 7. For example, the negative ozone tendency near 60E in phase 1 is consistent with the change of the positive ozone anomalies in phase 1 to the negative ozone anomalies in phase 2 (Fig. 7) there. In phases 3 and 7 the ozone tendencies (0-120E and 120E-60W) are in phase with the ozone anomalies, explaining the enhanced ozone anomalies in phase 4 and 8 and the pause of the eastward movement (Fig. 7). The similarity of the patterns of the total ozone tendency and that due to advection suggests that advection is the driving force for the ozone change during the MJO (The spatial correlation coefficient is 0.74, 0.65, 0.72, 0.70 for phase 1, 3, 5, 7 respectively, which are significant at the 95% confidence level). However, in a few specific locations other processes dominate (e.g., chemistry near 90W for phase 1 and phase 5). Overall, the ozone generally decreases where there is an upward motion (negative omega), and increases where there is downward motion (positive omega). However, it is clear that omega alone does not give the complete story. The advective ozone flux also depends on vertical ozone gradients (see Fig. 1) and horizontal advection. As stated previously it is very difficult to separate the horizontal and vertical transport from the advection in the current model simulation.

Net chemistry effect is significantly smaller in magnitude than advection, despite the importance of lightning in determining the magnitude of the MJO-

related tropospheric ozone anomalies (section 4.3, Fig. 7). The explanation of this apparent paradox lies in the fact that lightning increases both the vertical and horizontal gradients of ozone (compare Fig. 3a with Fig. 1a). The increased vertical and horizontal ozone gradients enhance ozone advection, the largest term driving the MJO-related tropospheric ozone anomalies (Fig. 8). The deep convective transport is small compared with the advective transport. Shallow convection and vertical diffusion are negligible compared with the previous three terms, consistent with Zhang and Mu (2005) that shallow convection in the composite MJO cycle is very weak (their Fig. 12b).

4.5 MJO Chemical Variability

Fig. 9 shows the percentage variability of ozone and OH related to the MJO. Variability of OH and O_3 due to the MJO generally ranges from 25-40% of the total variability (from daily to interannual) across much of the tropics and throughout the depth of the troposphere. The maximum ozone variability caused by the MJO reaches 47% of the total variability near 60E and 130E at 200 hPa and 80E at 500 hPa. The relative variability of OH generally resembles that of ozone reaching a maximum of 40%, but is generally somewhat weaker. Generally, the three regions where the highest intraseasonal variability of ozone and OH occurs (60E-90E, 150E, and 120W-90W) appear to be loosely related to the intraseasonal variability of lightning (Fig. 9c).

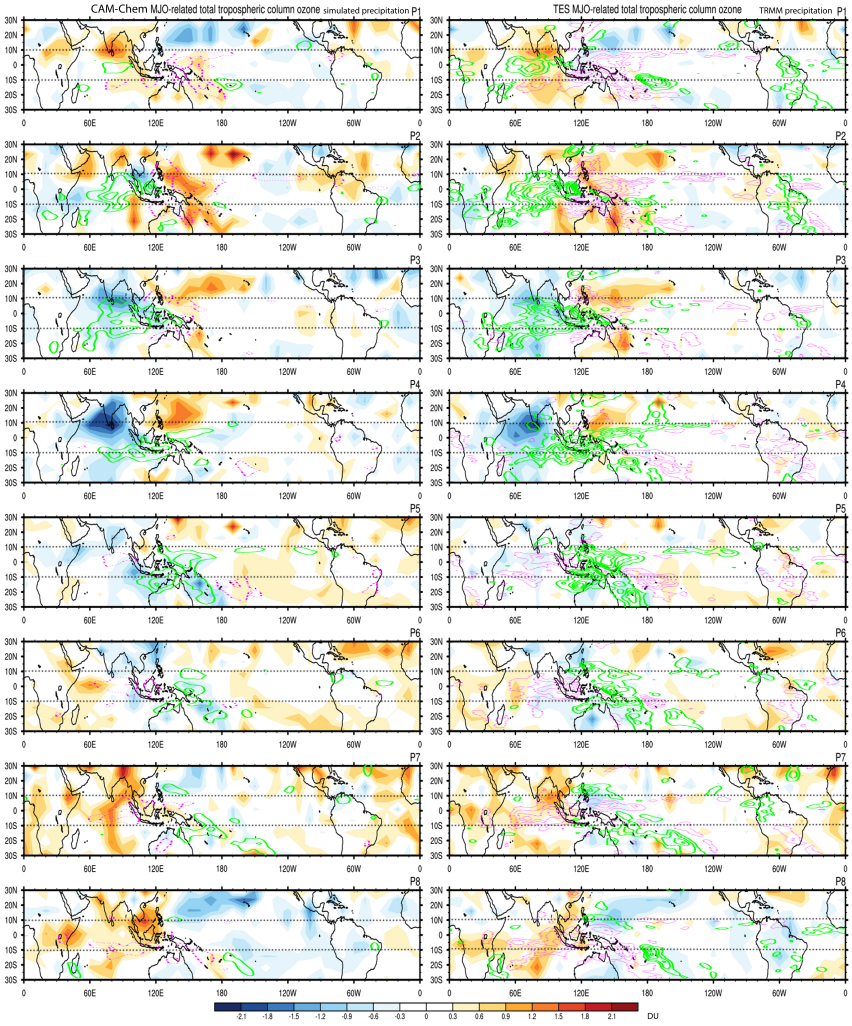

Figure 4.2: Left: Composite life cycle (phase 1 to 8) of the MJO-related total tropospheric column (s) ozone (color shades, in DU) for CAM-chem (with the TES operator applied) with precipitation (lines,green as positive and purple as negative); Right: Composite life cycle of the MJO-related TTC ozone for TES (color shades, in DU) with TRMM precipitation (lines, green as positive and purple as negative) for 30S to 30N. The precipitation is contoured from -3 to 3 mm/day with 0.5 mm/day interval.

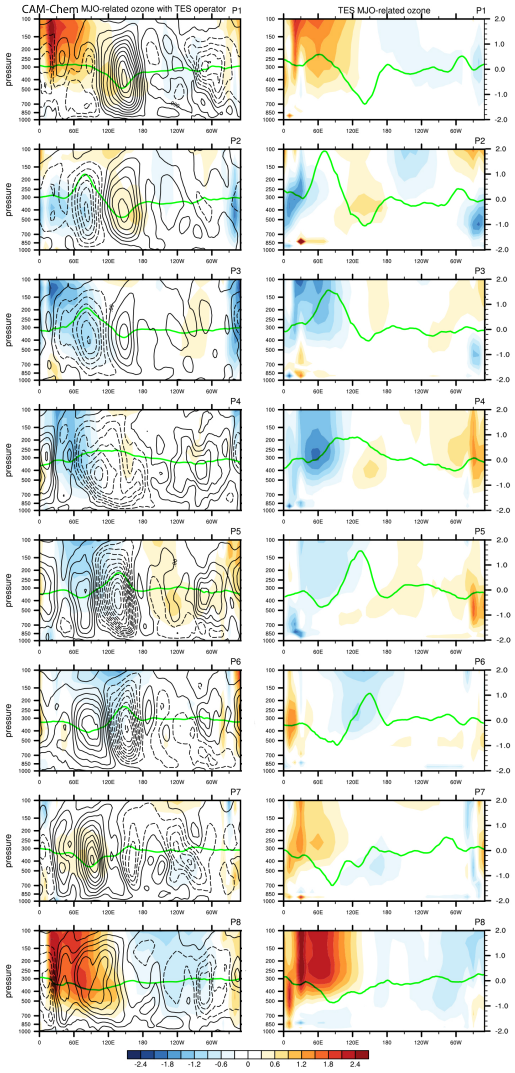

Figure 4.3: Left: MJO-related ozone (color shades) for CAM-chem (with the TES operator applied) with GEOS-5 vertical velocity (black lines, dashed as negative and solid as positive) and precipitation (green lines, in mm/day); Right: MJO-related ozone (color shades) for TES (color shades) with TRMM precipitation (green lines, in mm/day).

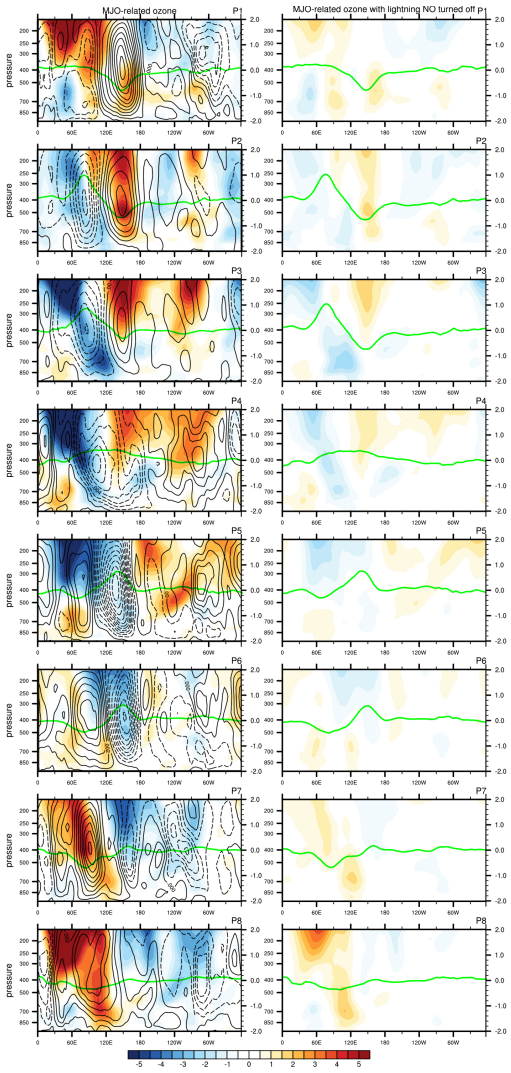

Figure 4.4: MJO-related ozone anomalies (color shades, in ppb) for the control run (left) and the lightning NOx turned off run (right) without applying the TES operator, with the simulated precipitation anomalies (lines, in mm/day).

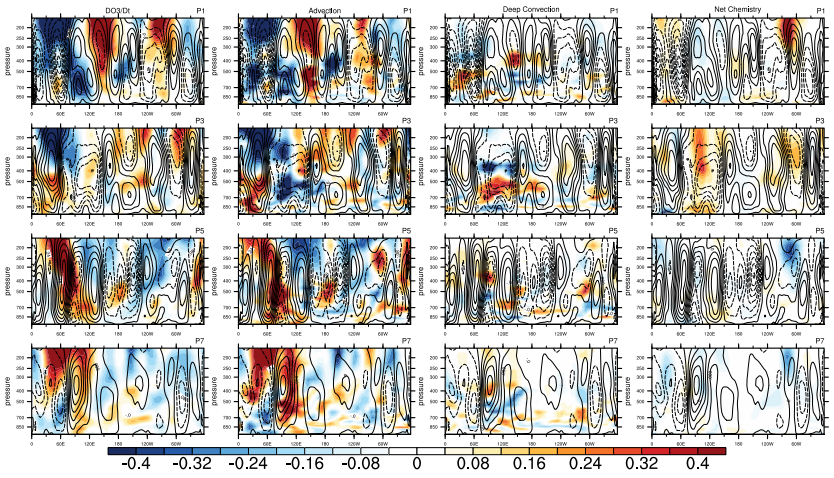

Figure 4.5: MJO-related tendency ($\left(\frac{\partial O_3}{\partial t}\right)$, $\left(\frac{\partial O_3}{\partial t}\right)_{advection}$, $\left(\frac{\partial O_3}{\partial t}\right)_{deepconvection}$, $\left(\frac{\partial O_3}{\partial t}\right)_{chemistry}$, color shades, in ppb/day) with vertical velocities (lines, dashed as negative and solid as positive).

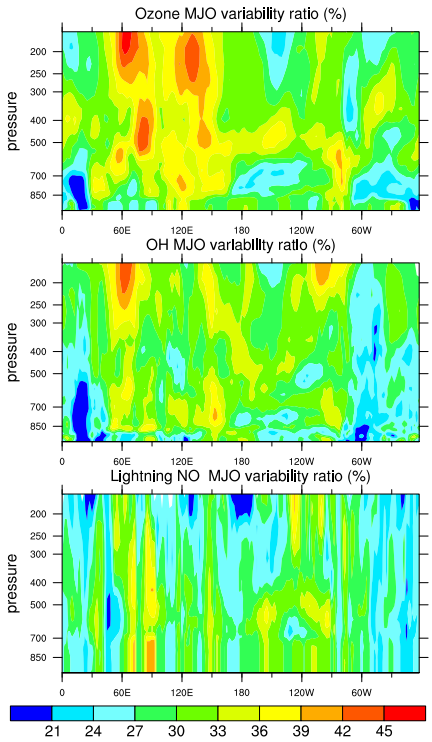

Figure 4.6: MJO variability ratio (given in percentage) for ozone, OH and lightning NO.

CHAPTER 5

CONCLUSIONS

The role of the MJO in total column ozone has been discussed before, but its connection with the tropospheric column ozone in the equatorial region in both model and observation has yet to be investigated in detail. This is the first study that documents the equatorial MJO-related tropospheric ozone oscillation in both a chemical transport model and satellite observations. We find the model when driven by analyzed meteorology can adequately simulate the MJO-related tropospheric ozone anomalies as measured from satellite. The MJO contributes substantially to the variability of both OH and ozone across the tropics, about 25-40% but is up to 50% in selected regions.

CAM-chem is able to qualitatively reproduce the equatorial ozone climatology during boreal winter (The simulated ozone distribution with the TES averaging kernel applied and the satellite ozone distribution are highly correlated, with the spatial correlation coefficient of 0.84 from 200 hPa to surface). However, there are some deficiencies for the CAM-chem model simulation. For example, CAM-chem generally has a positive ozone bias of (~ 10 ppb) compared with TES with the largest bias located near 120-60 W. In the middle troposphere over the western Pacific (near 150E) the CAM-chem simulated ozone is less than the measured (~ 10 ppb). In the boundary layer, the CAM-chem is positively biased compared with TES. Lightning plays an important role in determining the climatological mean ozone. The difference between the control run model simulation and the model simulation with no lightning reaches up to 30 ppb in the upper troposphere near 60W and 10E (where the lightning NOx source is maximum). Lightning also increases the vertical and horizontal ozone gradients

compared to a simulation with no lightning.

In the boreal winter (November through April) climatologically high ozone concentrations are evident throughout most of the depth of the troposphere in both simulation and measurements from 30-60E; near 150E low ozone concentrations are evident in both. The low ozone concentrations near 150E occur through out the depth of the troposphere. They occur in association with a precipitation maximum and have been attributed to convection transporting low ozone concentrations from the boundary layer to the upper troposphere (Lelieveld et al., 2001), although in the simulation large-scale vertical advection is also important. The TES operator does not dramatically change the simulated climatological ozone distribution, although the result of applying the TES operator is to increase the boundary layer ozone and reduce the upper tropospheric ozone (near 180E).

The behavior of TTC ozone on the intraseasonal time scale is different from that of the total column ozone, especially in the equatorial region. The TTC ozone anomalies related to MJO (~ 2 DU) propagate eastward in the tropical region, with the signal maximizing in the Indian Ocean and the west Pacific in association with the largest vertical velocities. Significantly, the magnitude of MJO-related TTC ozone anomalies in the equatorial region is comparable to that in the subtropics. The TTC ozone anomalies move eastward with the eastward propagation of the large-scale MJO convective and dynamical signals. The patterns of model simulated and satellite measured TTC ozone anomalies and precipitation anomalies for the eight phases of the MJO are in overall agreement with the TES measurements both in the tropics and the subtropics (Fig. 5, 6), although the magnitude and the spatial scale of the precipitation anomalies in

CAM-chem are smaller than that observed using TRMM.

While the vertical resolution of TES in the troposphere is somewhat limited, when the TES operator is applied to the simulated ozone profiles the modeled and measured ozone anomalies generally agree in pattern and amplitude with height, with the average spatial correlation coefficient as 0.63 for the 8 phases. The ozone signal in the eastern portion of the equatorial domain propagates very little but is generally out of phase with the signal in the western portion of the equatorial domain. However, the MJO in the CAM-chem looks somewhat different without the averaging kernel applied. The TES operator flattens the ozone anomalies and decreases the magnitude to ~ 50%, and also changes the relative magnitude of the signal between phases. When the TES operator is applied only phases 1 and 8 are particularly enhanced, while the raw model output suggests the ozone signal is not considerably weaker during the other phases.

Large-scale advection explains most of the simulated ozone changes associated with the MJO. While many of the simulated changes appear related to the vertical velocity perturbations, the correlation between the advective ozone tendency and omega is generally small. Lightning NOx emissions enhance the amplitude of the MJO ozone anomalies by about a factor of 5 over a simulation without lightning NOx emissions, despite the fact that changes in the chemical tendency associated with the MJO are small. Lightning increases the horizontal and vertical ozone gradients and thus increasing the advective ozone anomalies.

The tropics represent an important, but often overlooked region, in the atmospheric processing of chemical constituents. Most chemistry transport models

are only given a cursory evaluation in the tropics. The equatorial MJO in ozone represents up to 47% of the variability of equatorial ozone. We have shown the signal is mostly due to large-scale atmospheric circulations allowing it to be represented in coarse scale models, and we also have shown a model simulation driven by analyzed winds is able to adequately represent the equatorial MJO. However, the ability of climate GCMs to represent the equatorial MJO in ozone is not well known.

BIBLIOGRAPHY

Andreae, M. O. and Merlet, P.: Emission of trace gases and aerosols from biomass burning, Global biogeochemical cycles, 15, 955–966, 2001.

Baughcum, S., Henderson, S., and Sutkus, D.: Scheduled civil aircraft emission inventories projected for 2015: Database development and analysis, NASA Contract. Rep NASA CR, pp. 1998–207 638, 1998.

Baughcum, S. L., Tritz, T. G., Henderson, S. C., and Pickett, D. C.: Scheduled civil aircraft emission inventories for 1992: Database development and analysis, National Aeronautics and Space Administration, Langley Research Center, 1996.

Beer, R.: TES on the Aura mission: Scientific objectives, measurements, and analysis overview, IEEE Transactions on Geoscience and remote sensing, 44, 1102–1105, 2006.

Beer, R., Glavich, T. A., and Rider, D. M.: Tropospheric emission spectrometer for the Earth Observing Systems Aura satellite, Applied optics, 40, 2356–2367, 2001.

Bowman, K. W., Rodgers, C. D., Kulawik, S. S., Worden, J., Sarkissian, E., Osterman, G., Steck, T., Lou, M., Eldering, A., Shephard, M., et al.: Tropospheric emission spectrometer: Retrieval method and error analysis, Geoscience and Remote Sensing, IEEE Transactions on, 44, 1297–1307, 2006.

Bowman, K. W., Jones, D. B. A., Logan, J. A., Worden, H., Boersma, F., Chang, R., Kulawik, S., Osterman, G., Hamer, P., and Worden, J.: The zonal structure of tropical O_3 and CO as observed by the Tropospheric Emission Spectrometer in November 2004 Part 2: Impact of surface emissions on O_3 and its precursors,

Atmospheric Chemistry and Physics, 9, 3563–3582, doi:10.5194/acp-9-3563-2009, URL http://www.atmos-chem-phys.net/9/3563/2009/, 2009.

Cooper, M. J., Martin, R. V., Livesey, N. J., Degenstein, D. A., and Walker, K. A.: Analysis of satellite remote sensing observations of low ozone events in the tropical upper troposphere and links with convection, Geophysical Research Letters, 40, 3761–3765, 2013.

Doherty, R., Stevenson, D., Collins, W., and Sanderson, M.: Influence of convective transport on tropospheric ozone and its precursors in a chemistry-climate model, Atmospheric Chemistry and Physics, 5, 3205–3218, 2005.

Eldering, A., Kulawik, S. S., Worden, J., Bowman, K., and Osterman, G.: Implementation of cloud retrievals for TES atmospheric retrievals: 2. Characterization of cloud top pressure and effective optical depth retrievals, Journal of Geophysical Research: Atmospheres (1984–2012), 113, 2008.

Emmons, L., Walters, S., Hess, P., Lamarque, J.-F., Pfister, G., Fillmore, D., Granier, C., Guenther, A., Kinnison, D., Laepple, T., et al.: Description and evaluation of the Model for Ozone and Related chemical Tracers, version 4 (MOZART-4), Geoscientific Model Development, 3, 43–67, 2010.

Folkins, I. and Martin, R. V.: The vertical structure of tropical convection and its impact on the budgets of water vapor and ozone., Journal of the atmospheric sciences, 62, 2005.

Folkins, I., Braun, C., Thompson, A. M., and Witte, J.: Tropical ozone as an indicator of deep convection, Journal of Geophysical Research: Atmospheres (1984–2012), 107, ACH–13, 2002.

Garcia, R., Marsh, D., Kinnison, D., Boville, B., and Sassi, F.: Simulation of secular trends in the middle atmosphere, 1950–2003, Journal of Geophysical Research: Atmospheres (1984–2012), 112, 2007.

Granier, C., Lamarque, J., Mieville, A., Muller, J., Olivier, J., Orlando, J., Peters, J., Petron, G., Tyndall, G., and Wallens, S.: POET, a database of surface emissions of ozone precursors, 2005.

Guenther, A., Karl, T., Harley, P., Wiedinmyer, C., Palmer, P., and Geron, C.: Estimates of global terrestrial isoprene emissions using MEGAN (Model of Emissions of Gases and Aerosols from Nature)., Atmospheric Chemistry & Physics, 6, 2006.

Hack, J. J., Caron, J. M., Yeager, S. G., Oleson, K. W., Holland, M. M., Truesdale, J. E., and Rasch, P. J.: Simulation of the global hydrological cycle in the CCSM Community Atmosphere Model version 3 (CAM3): Mean features., Journal of climate, 19, 2006.

Hendon, H. H. and Salby, M. L.: The life cycle of the Madden-Julian oscillation, Journal of the Atmospheric Sciences, 51, 2225–2237, 1994.

Holtslag, A. and Boville, B.: Local versus nonlocal boundary-layer diffusion in a global climate model, Journal of Climate, 6, 1825–1842, 1993.

Houghton, J. T., Ding, Y., Griggs, D. J., Noguer, M., van der LINDEN, P. J., Dai, X., Maskell, K., and Johnson, C.: Climate change 2001: the scientific basis, vol. 881, Cambridge university press Cambridge, 2001.

Huffman, G. J., Adler, R. F., Bolvin, D. T., Gu, G., Nelkin, E. J., Bowman, K. P., Hong, Y., Stocker, E. F., and Wolff, D. B.: The TRMM Multisatellite Precipi-

tation Analysis (TMPA): Quasi-global, multiyear, combined-sensor precipitation estimates at fine scales., Journal of Hydrometeorology, 8, 2007.

Jee-Hoon, J., Baek-Min, K., Chang-Hoi, H., and Yeon-Hee, N.: Systematic Variation in Wintertime Precipitation in East Asia by MJO-Induced Extratropical Vertical Motion., Journal of Climate, 21, 788 – 801, URL http://search.ebscohost.com/login.aspx?direct=truedb=aphAN=29987826s 2008.

Jourdain, L., Worden, H., Worden, J., Bowman, K., Li, Q., Eldering, A., Kulawik, S., Osterman, G., Boersma, K., Fisher, B., et al.: Tropospheric vertical distribution of tropical Atlantic ozone observed by TES during the northern African biomass burning season, Geophysical Research Letters, 34, 2007.

Kulawik, S. S., Worden, H., Osterman, G., Luo, M., Beer, R., Kinnison, D. E., Bowman, K. W., Worden, J., Eldering, A., Lampel, M., et al.: TES atmospheric profile retrieval characterization: An orbit of simulated observations, Geoscience and Remote Sensing, IEEE Transactions on, 44, 1324–1333, 2006.

Labrador, L., Kuhlmann, R. v., and Lawrence, M.: The effects of lightning-produced NO x and its vertical distribution on atmospheric chemistry: Sensitivity simulations with MATCH-MPIC, Atmospheric Chemistry and Physics, 5, 1815–1834, 2005.

Lacis, A. A., Wuebbles, D. J., and Logan, J. A.: Radiative forcing of climate by changes in the vertical distribution of ozone, Journal of Geophysical Research: Atmospheres (1984–2012), 95, 9971–9981, 1990.

Lamarque, J., Emmons, L., Hess, P., Kinnison, D. E., Tilmes, S., Vitt, F., Heald, C., Holland, E. A., Lauritzen, P., Neu, J., et al.: CAM-chem: Description and eval-

uation of interactive atmospheric chemistry in the Community Earth System Model, Geosci. Model Dev, 5, 369–411, 2012.

Lau, W. K. and Waliser, D. E.: El Nino southern oscillation connection, in: Intraseasonal Variability in the Atmosphere-Ocean Climate System, pp. 297–334, Springer, 2012.

Lawrence, M., Chameides, W., Kasibhatla, P., Levy II, H., and Moxim, W.: Lightning and atmospheric chemistry: The rate of atmospheric NO production, Handbook of atmospheric electrodynamics, 1, 189–202, 1995.

Lawrence, M. G., von Kuhlmann, R., Salzmann, M., and Rasch, P. J.: The balance of effects of deep convective mixing on tropospheric ozone, Geophysical research letters, 30, 2003.

Lelieveld, J. and Crutzen, P. J.: Role of deep cloud convection in the ozone budget of the troposphere, Science, 264, 1759–1761, 1994.

Lelieveld, J. and Dentener, F. J.: What controls tropospheric ozone?, Journal of Geophysical Research: Atmospheres, 105, 3531–3551, doi:10.1029/1999JD901011, URL http://dx.doi.org/10.1029/1999JD901011, 2000.

Lelieveld, J. o., Crutzen, P., Ramanathan, V., Andreae, M., Brenninkmeijer, C., Campos, T., Cass, G., Dickerson, R., Fischer, H., De Gouw, J., et al.: The Indian Ocean experiment: widespread air pollution from South and Southeast Asia, Science, 291, 1031–1036, 2001.

Li, K.-F., Tian, B., Waliser, D., Schwartz, M., Neu, J., Worden, J., and Yung, Y.: Vertical structure of MJO-related subtropical ozone variations from MLS, TES, and SHADOZ data, Atmospheric Chemistry and Physics, 12, 425–436, 2012.

Li, K.-F., Tian, B., Tung, K.-K., Kuai, L., Worden, J. R., Yung, Y. L., and Slawski, B. L.: A link between tropical intraseasonal variability and Arctic stratospheric ozone, Journal of Geophysical Research: Atmospheres, 118, 4280–4289, 2013.

Logan, J. A., Prather, M. J., Wofsy, S. C., and McElroy, M. B.: Tropospheric chemistry: A global perspective, Journal of Geophysical Research: Oceans, 86, 7210–7254, doi:10.1029/JC086iC08p07210, URL http://dx.doi.org/10.1029/JC086iC08p07210, 1981.

Madden, R. A. and Julian, P. R.: Detection of a 40-50 day oscillation in the zonal wind in the tropical Pacific, Journal of the Atmospheric Sciences, 28, 702–708, 1971.

Madden, R. A. and Julian, P. R.: Description of global-scale circulation cells in the tropics with a 40-50 day period, Journal of the Atmospheric Sciences, 29, 1109–1123, 1972.

Martin, R. V., Jacob, D. J., Logan, J. A., Bey, I., Yantosca, R. M., Staudt, A. C., Li, Q., Fiore, A. M., Duncan, B. N., Liu, H., et al.: Interpretation of TOMS observations of tropical tropospheric ozone with a global model and in situ observations, Journal of Geophysical Research: Atmospheres (1984–2012), 107, ACH–4, 2002.

Mortlock, A. and Van Alstyne, R.: Military, Charter, Unreported Domestic Traffic and General Aviation 1976, 1984, 1992, and 2015 Emission Scenarios, National Aeronautics and Space Administration, Langley Research Center, 1998.

Nassar, R., Logan, J. A., Worden, H. M., Megretskaia, I. A., Bowman, K. W., Osterman, G. B., Thompson, A. M., Tarasick, D. W., Austin, S., Claude, H.,

et al.: Validation of Tropospheric Emission Spectrometer (TES) nadir ozone profiles using ozonesonde measurements, Journal of Geophysical Research: Atmospheres (1984–2012), 113, 2008.

Osterman, G., Kulawik, S., Worden, H., Richards, N., Fisher, B., Eldering, A., Shephard, M., Froidevaux, L., Labow, G., Luo, M., et al.: Validation of Tropospheric Emission Spectrometer (TES) measurements of the total, stratospheric, and tropospheric column abundance of ozone, Journal of Geophysical Research: Atmospheres (1984–2012), 113, 2008.

Pickering, K. E., Wang, Y., Tao, W.-K., Price, C., and Müller, J.-F.: Vertical distributions of lightning NOx for use in regional and global chemical transport models, Journal of Geophysical Research: Atmospheres (1984–2012), 103, 31 203–31 216, 1998.

Price, C. and Rind, D.: A simple lightning parameterization for calculating global lightning distributions, Journal of Geophysical Research: Atmospheres (1984–2012), 97, 9919–9933, 1992.

Price, C., Penner, J., and Prather, M.: NOx from lightning: 1. Global distribution based on lightning physics, Journal of Geophysical Research: Atmospheres (1984–2012), 102, 5929–5941, 1997.

Randel, W. J. and Jensen, E. J.: Physical processes in the tropical tropopause layer and their roles in a changing climate, Nature Geoscience, 6, 169–176, 2013.

Richards, N. A., Osterman, G. B., Browell, E. V., Hair, J. W., Avery, M., and Li, Q.: Validation of Tropospheric Emission Spectrometer ozone profiles with aircraft

observations during the Intercontinental Chemical Transport Experiment–B, Journal of Geophysical Research: Atmospheres (1984–2012), 113, 2008.

Rodgers, C. D. et al.: Inverse methods for atmospheric sounding: Theory and practice, vol. 2, World scientific Singapore, 2000.

Sauvage, B., Martin, R. V., Van Donkelaar, A., and Ziemke, J.: Quantification of the factors controlling tropical tropospheric ozone and the South Atlantic maximum, Journal of Geophysical Research: Atmospheres (1984–2012), 112, 2007.

Sperber, K. R.: Propagation and the vertical structure of the Madden-Julian Oscillation, Monthly Weather Review, 131, 3018–3037, 2003.

Sutkus, D. J., Baughcum, S. L., and DuBois, D. P.: Scheduled civil aircraft emission inventories for 1999: database development and analysis, National Aeronatics and Space Administration (NASA) Glenn Research Center, Contract NAS1-20341. NASA/CR-2001-211216, 2001.

Thompson, A. M., Witte, J. C., Oltmans, S. J., Schmidlin, F. J., Logan, J. A., Fujiwara, M., Kirchhoff, V. W., Posny, F., Coetzee, G. J., Hoegger, B., et al.: Southern Hemisphere Additional Ozonesondes (SHADOZ) 1998–2000 tropical ozone climatology 2. Tropospheric variability and the zonal wave-one, Journal of Geophysical Research: Atmospheres (1984–2012), 108, 2003.

Tian, B. and Waliser, D. E.: Chemical and biological impacts, Intraseasonal Variability in the Atmosphere–Ocean Climate System, 2, 569–585, 2011.

Tian, B., Yung, Y., Waliser, D., Tyranowski, T., Kuai, L., Fetzer, E., and Irion, F.: Intraseasonal variations of the tropical total ozone and their connection to the Madden-Julian Oscillation, Geophysical Research Letters, 34, 2007.

Tian, B., Waliser, D. E., Fetzer, E. J., and Yung, Y. L.: Vertical Moist Thermodynamic Structure of the Madden–Julian Oscillation in Atmospheric Infrared Sounder Retrievals: An Update and a Comparison to ECMWF Interim Re-Analysis., Monthly Weather Review, 138, 2010.

Tian, B., Waliser, D. E., Kahn, R. A., and Wong, S.: Modulation of Atlantic aerosols by the Madden-Julian Oscillation, Journal of Geophysical Research: Atmospheres (1984–2012), 116, 2011.

van der Werf, G. R., Randerson, J. T., Giglio, L., Collatz, G. J., Kasibhatla, P. S., and Arellano Jr, A.: Interannual variability in global biomass burning emissions from 1997 to 2004, Atmospheric Chemistry and Physics, 6, 3423–3441, 2006.

Virts, K. S., Thornton, J. A., Wallace, J. M., Hutchins, M. L., Holzworth, R. H., and Jacobson, A. R.: Daily and intraseasonal relationships between lightning and NO2 over the Maritime Continent, Geophysical Research Letters, 38, 2011.

Virts, K. S., Wallace, J. M., Hutchins, M. L., and Holzworth, R. H.: Diurnal Lightning Variability over the Maritime Continent: Impact of Low-Level Winds, Cloudiness, and the MJO., Journal of the Atmospheric Sciences, 70, 2013.

Wheeler, M. C. and Hendon, H. H.: An all-season real-time multivariate MJO index: Development of an index for monitoring and prediction., Monthly Weather Review, 132, 2004.

Worden, H., Logan, J., Worden, J., Beer, R., Bowman, K., Clough, S., Eldering, A., Fisher, B., Gunson, M., Herman, R., et al.: Comparisons of Tropospheric Emis-

sion Spectrometer (TES) ozone profiles to ozonesondes: Methods and initial results, Journal of Geophysical Research: Atmospheres (1984–2012), 112, 2007.

Worden, H. M., Bowman, K. W., Worden, J. R., Eldering, A., and Beer, R.: Satellite measurements of the clear-sky greenhouse effect from tropospheric ozone, Nature Geoscience, 1, 305–308, 2008.

Worden, J., Kulawik, S. S., Shephard, M. W., Clough, S. A., Worden, H., Bowman, K., and Goldman, A.: Predicted errors of tropospheric emission spectrometer nadir retrievals from spectral window selection, Journal of Geophysical Research: Atmospheres (1984–2012), 109, doi:10.1029/2004JD004522, 2004.

Zhang, C.: Madden-julian oscillation, Reviews of Geophysics, 43, 2005.

Zhang, G. J. and McFarlane, N. A.: Sensitivity of climate simulations to the parameterization of cumulus convection in the Canadian Climate Centre general circulation model, Atmosphere-Ocean, 33, 407–446, 1995.

Zhang, G. J. and Mu, M.: Simulation of the Madden–Julian Oscillation in the NCAR CCM3 Using a Revised Zhang–McFarlane Convection Parameterization Scheme., Journal of climate, 18, 2005.

Ziemke, J. and Chandra, S.: A Madden-Julian Oscillation in tropospheric ozone, Geophysical research letters, 30, 2003.

Ziemke, J., Chandra, S., Schoeberl, M., Froidevaux, L., Read, W., Levelt, P., and Bhartia, P.: Intra-seasonal variability in tropospheric ozone and water vapor in the tropics, Geophysical Research Letters, 34, 2007.

Ziemke, J., Joiner, J., Chandra, S., Bhartia, P., Vasilkov, A., Haffner, D., Yang, K., Schoeberl, M., Froidevaux, L., and Levelt, P.: Ozone mixing ratios inside trop-

ical deep convective clouds from OMI satellite measurements, Atmospheric Chemistry and Physics, 9, 573–583, 2009.